Growing $LaRuO_3/LaAlO_3$ Quantum Anomalous Hall Insulators

Lawrence Qiu[1], Evan Krysko[2], and Darrell G. Schlom[2]

[1]Department of Electrical and Computer Engineering, Tufts University
[2]Department of Materials Science and Engineering, Cornell University

PARADIM REU 2024

Abstract

Efforts to explain the Hall family of effects led to the nascent theory of topological materials. Materials exhibiting these properties are of significant theoretical and practical interest, showing potential in industries like quantum and classical computing, data storage, and power electronics. Quantum anomalous Hall insulators are a relatively recent addition to this family, describing materials with quantized Hall resistance without an applied magnetic field. Previous studies predicted that a lanthanum ruthenate/lanthanum aluminate sandwich heterostructure will exhibit this effect. We formulate and partially realize a plan to fabricate such a structure using molecular-beam epitaxy.

1 Introduction

Since the original discovery of the Hall effect by Edwin Hall in the 19^{th} century, numerous variations have been proposed to explain increasing exotic phenomena. These include the anomalous Hall effect, the spin Hall effect, the integer quantum Hall effect, the fractional quantum Hall effect, and so on. As experimental efforts yielded novel results, theory advanced in lockstep, most notably through the development of the theory of topological materials. Here, ideas from the mathematical field of topology are applied to analyze material band structure, resulting in the first descriptions of the novel phenomena.

The quantum anomalous Hall effect (QAHE) can be seen as the combination of the anomalous Hall effect and the quantum Hall effect[4]. The anomalous Hall effect causes a deviation from the linear relationship between the magnetic field strength and Hall conductance as seen in the classical Hall effect. Despite being the first variant of the Hall effect to be discovered, the explanation of the effect is involved and was subjected to intense historical debate[6]. Today, several mechanisms causing the anomalous Hall effect are known. They are classified into two types: intrinsic mechanisms, which depend on the band structure of the pure material, and extrinsic mechanisms, which result from defects in real world materials. Together, these effects contribute an additional factor to the Hall conductance in certain materials.

The quantum Hall effect also causes a deviation from the classical Hall effect relationship, manifesting as a quantized Hall resistance[2]. It occurs under strong magnetic fields and low temperatures, which result in highly degenerate energy bands known as Landau levels. As the magnetic field rises, the Landau levels move apart and increase in energy until only a limited number of levels are below the Fermi energy. Each level contributes a significant number of carriers to the total carrier count, and as the Landau levels move up further, the carrier count drops in steps, with the step size corresponding to the degeneracy of each level. Since the carrier count is related to the Hall resistance, the Hall resistance also drops in steps, resulting in the quantized Hall resistance. Specifically, the following equation describes the Hall resistance with the number of remaining Landau levels, which matches the values at each step in the graph plotting Hall resistance against magnetic field strength as shown in Figure 1.

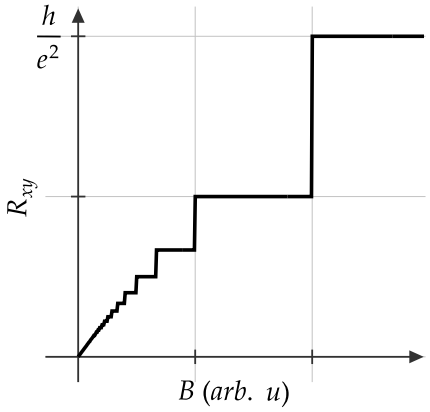

Figure 1. Plot of Hall resistance against magnetic field strength when exhibiting the quantum Hall effect. The Hall resistance rises in steps corresponding to values of $\frac{h}{e^2 v}$.

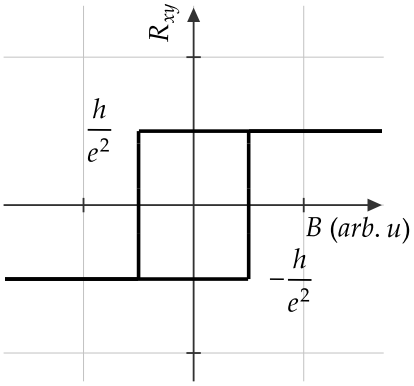

Figure 2. Plot of Hall resistance against magnetic field strength when exhibiting the quantum anomalous Hall effect. The Hall resistance takes values of $\pm\frac{h}{e^2}$, with doublevaluedness showing hysteresis.

$$R_{xy} = \frac{h}{e^2 v}, \quad v = 1, 2, 3, \cdots$$

In the quantum anomalous Hall effect, the two effects combine, resulting in a quantized hall resistance even without an external magnetic field. Specifically, the Hall resistance is expected to take values of $\pm\frac{h}{e^2}$, or about $\pm 25.8\text{k}\Omega$. Figure 2 shows the relationship between applied magnetic field and Hall resistance; hysteresis allows the effect to be symmetric across the transverse axis while still taking a non-zero value.

Understanding of the effect is relatively recent: empirical observation of the quantum anomalous Hall effect was achieved only in 2014 by Nagaosa et al.[4], and research into its nuances continues to this day. Of interest to our project are two theoretical predictions by Köksal et al. and Guo et al.[5, 3]. These studies used density functional theory (DFT) to predict that QAHE states will occur in perovskite sandwich structures. Specifically, both studies suggest that the QAHE will arise in a lanthanum ruthenate (LRO) and lanthanum aluminate (LAO) sandwich heterostructure, as shown in Figure 3. The structure consists of two monolayers of LRO with one monolayer of LAO on top and bottom. Each layer must be (111)-oriented and strained to the neodymium gallate (NGO) substrate. Our primary goal is to realize this structure and empirically observe the effect.

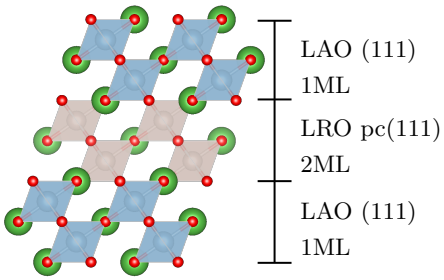

Figure 3. The lanthanum ruthenate and lanthanum aluminate sandwich heterostructure predicted to exhibit the QAHE. Two monolayers of pc(111) LRO are sandwiched between a single monolayer of (111) LAO.

2 Methods

2.1 Molecular-Beam Epitaxy

Our chosen method of fabricating the $LaRuO_3/LaAlO_3$ heterostructure is through molecular-beam epitaxy (MBE). MBE is an established method of depositing thin films of materials and material structures on substrates. It is often compared to atomic spray painting: constituents of the target material are heated and allowed to sublime, forming beams of material that deposit onto the substrate, similarly to how in spray-painting, beams of atomized paint are formed that deposit onto a surface.

The versatility of MBE can be attributed to the countless variables that can be tuned to achieve a

suitable film. These include the fluxes of each constituent material, the temperature of the substrate, the set of constituents to use (such as whether to use the elemental form or an oxide), pressure and type of oxidizer (oxygen, ozone, or a mix), choice of substrate, and more. However, the availability of so many parameters to tune also complicates the process of optimizing growth conditions for a particular film.

2.2 Potential Growth Difficulties

We anticipate that our structure will be especially challenging to grow due to strain, the higher (111)-orientation surface energy, compatibility between LRO and LAO, and the precise monolayer count needed to realize the QAHE. Firstly, both the LRO and the LAO layers need to be strained to the NGO substrate. For LRO this is a compressive 2.03% strain and for LAO this is a tensile 1.78% strain. High strain causes dislocations and undesirable growth patterns like islanding, requiring finely tuned growth parameters to achieve an acceptable film. Secondly, the (111)-orientation has higher surface energy. Surface energy is defined as the energy required to create a surface and primarily depends on the bonds broken by a surface. Since the set of bonds broken by different surfaces differs, the surface energy also differs. Generally, (111)-oriented surfaces have higher surface energy than (100)-oriented surfaces for perovskites. Eglitis et al. calculated the surface energy for several perovskites under each orientation and found that they all follow this trend[1]. As thermal fluctuations may cause a smooth (111)-oriented surface to reorient into lower-energy surface structures, increasing roughness, finely tuned growth parameters are necessary to obtain optimal growth. Thirdly, the growth conditions must be compatible with both LRO and LAO because changing growth conditions significantly between each layer would make the growth more challenging. Lastly, a precise monolayer count is needed to realize the sandwich structure accurately and to observe the QAHE. This would require accurate shutter timing to avoid over or under exposing the substrate to flux.

2.3 Plan

Because we expect that immediately attempting to grow the final structure will be challenging due to the previously mentioned difficulties, we instead simplified the elements of the final structure, breaking it apart into separate steps where we introduce each individual difficulty one-by-one. This approach simplifies the process of optimizing growth conditions. Our five-step plan is as follows:

1. Optimize growth of (100) LRO & LAO on lattice matched substrate
2. Grow strained (100) LRO & LAO w/ pc(100) NGO substrate
3. Move to (111) LRO & LAO on pc(111) NGO substrate
4. Grow LRO/LAO heterostructures on pc(111) NGO
5. Finally, grow structure as described and measure QAHE

After growing each sample and before advancing to the next step, we plan to characterize and determine the quality of the sample using X-ray diffraction (XRD), atomic force microscopy (AFM), reflection high-energy electron diffraction (RHEED), reciprocal space mapping (RSM), and transport measurements.

3 Results and Discussion

3.1 Growth Condition Trends

3.1.1 Lanthanum Aluminate

The LAO growth series is visualized in Figure 4. The two growth variables we primarily varied to optimize the film quality are the substrate temperature and the aluminum flux. We observed the following trends as we adjusted the variables. If the substrate temperature is too high, we observe surface roughening due to thermal rearrangement away from the high surface energy (111) surface. If the substrate temperature is too low, we find that our film becomes amorphous. If the aluminum flux is too high, we observe unwanted peaks in the XRD suggesting aluminum content, and if the aluminum flux is too low, we observe an abnormal RHEED pattern suggesting excessive lanthanum.

3.1.2 Lanthanum Ruthenate

Similarly, the LRO growth series is visualized in Figure 5. We primarily varied the substrate temperature and the ruthenium flux to optimize our film, and we observed the following trends as we adjusted the variables. The substrate temperature relationship is similar: we expect surface roughening at high substrate temperatures and amorphous films at low substrate temperature. However, because lanthanum ruthenate is adsorption controlled, excessive ruthenium flux does not significantly deteriorate the film. At low ruthenium fluxes, we observe lanthanum oxide and ruthenium vacancies.

3.2 Selected Samples

From our growth series, we selected the following set of notable samples:

3.2.1 LAO36

Sample LAO36 represents our best lanthanum aluminate sample strained on pc(111) NGO. It was grown at 600 °C with a stoichiometric aluminum to lanthanum flux ratio. Figure 6a shows the XRD scan; the sharp film peaks at the expected locations suggest good film quality. AFM imaging also shows low surface roughness with an RMS of 0.2nm, as indicated in Figure 6c. Finally, the RSM scan in 6b confirms that the film is strained to the substrate.

3.2.2 LRO34

Sample LRO34 represents our best lanthanum ruthenate sample grown on the lattice-matched pc(100) STO substrate. It was grown at substrate temperatures between 700 °C and 800 °C. The XRD scan in Figure 7a again suggests a good film due to sharp peaks at the expected locations. AFM imaging shown in Figure 7b indicates low surface roughness with an RMS of 0.25nm, although it is spotty. Finally, the RHEED images in Figure 7c shows the presence of spots on an arc, as expected, and Kikuchi lines, suggesting a crystalline film.

3.2.3 LRO39

Sample LRO39 represents our best lanthanum ruthenate sample strained on pc(100) NGO. It was grown at the substrate temperature of 700 °C. The XRD scan shown in Figure 8a suggests a good film and the RSM scan in Figure 8b confirms that the film is strained to the substrate. However, there are unexpected spots in the RHEED images in Figure 8c, suggesting that more progress is necessary.

3.2.4 LRO29/LAO35

Lastly, sample LRO29/LAO35 represents an early attempt at growing the LRO-on-LAO heterostructure. The LAO portion was grown with similar parameters as LAO36, and the LRO portion used the substrate temperature of 600 °C. The XRD scan shown in Figure 9a shows the LAO film peaks distinctly, but the LRO peaks are shifted away from their expected locations, potentially due to strain or non-stoichiometric phase. The AFM image shown in Figure 9b also indicates higher surface roughness with an RMS of 0.4nm.

4 Conclusions and Future Work

We created and particularly realized a plan to fabricate the lanthanum ruthenate/lanthanum aluminate sandwich heterostructure that is predicted to exbibit the quantum anomalous Hall effect. Notably, we tuned growth conditions for high quality lanthanum aluminate (111)-oriented films strained on pc(111) neodymium gallate, as well as lanthanum ruthenate (100)-oriented films strained on pc(100) neodymium gallate.

Our next steps are to continue with the remaining steps of our plan, namely finishing the optimization of strained pc(100) LRO, optimizing pc(111) LRO, growing the LRO-on-LAO heterostructure, and finally creating the original QAHE structure. To measure the QAHE on the final structure, we plan to fabricate a Hall bar pattern on our sample using the procedure described by Rodenbach et al.[7], working with a collaborator to perform microfabrication.

5 Acknowledgements

I am very grateful for my mentor Evan Krysko, who provided me with the opportunity to learn from and contribute to this project through the PARADIM REU program. Additionally, I would like to thank Vivek Anil, Evan Yilin Li, Anna Park, Jim Overhiser, Brenda Fisher, and my PI Darrell G. Schlom.

This project utilized the PARADIM facility, which is supported by the National Science Foundation under Cooperative Agreement No. DMR-2039380.

6 References

[1] Roberts I. Eglitis. Comparative First-Principles Calculations of $SrTiO_3$, $BaTiO_3$, $PbTiO_3$ and $CaTiO_3$ (001), (011) and (111) Surfaces. *Ferroelectrics*, 483(1):53–67, July 2015.

[2] M. O. Goerbig. Quantum Hall Effects, October 2009. arXiv:0909.1998 [cond-mat].

[3] Hongli Guo, Shruba Gangopadhyay, Okan Kksal, Rossitza Pentcheva, and Warren E. Pickett. Wide gap Chern Mott insulating phases achieved by design. *npj Quantum Materials*, 2(1):1–8, January 2017.

[4] Ke He, Yayu Wang, and Qi-Kun Xue. Quantum anomalous Hall effect. *National Science Review*, 1(1):38–48, March 2014.

[5] Okan Kksal and Rossitza Pentcheva. Chern and Z2 topological insulating phases in perovskite-derived 4d and 5d oxide buckled honeycomb lattices. *Scientific Reports*, 9(1):17306, November 2019.

[6] Naoto Nagaosa, Jairo Sinova, Shigeki Onoda, A. H. MacDonald, and N. P. Ong. Anomalous Hall effect. *Reviews of Modern Physics*, 82(2):1539–1592, May 2010.

[7] Linsey K. Rodenbach, Alireza R. Panna, Shamith U. Payagala, Ilan T. Rosen, Molly P. Andersen, Peng Zhang, Lixuan Tai, Kang L. Wang, Dean G. Jarrett, Randolph E. Elmquist, David B. Newell, David Goldhaber-Gordon, and Albert F. Rigosi. Metrological Assessment of Quantum Anomalous Hall Properties. *Physical Review Applied*, 18(3):034008, September 2022.

Appendix A Additional Figures

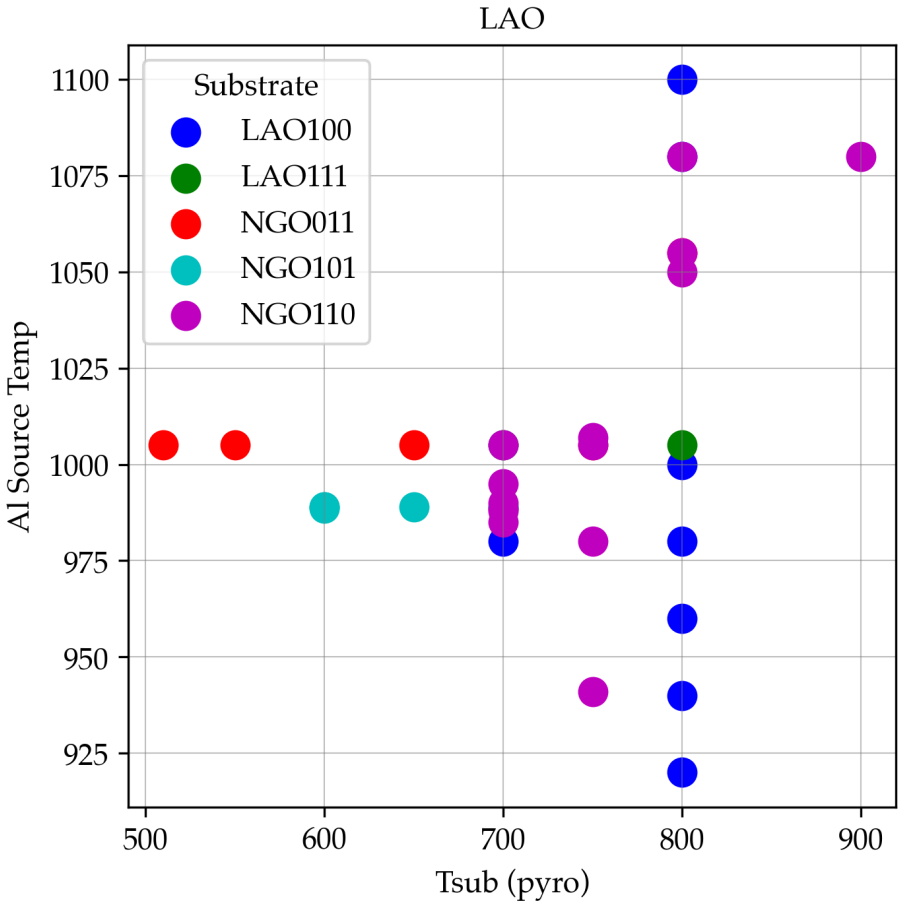

Figure 4. Scatter plot showing the LAO series of growths. Each point indicates a single growth with a particular substrate, substrate temperature, and aluminum source temperature.

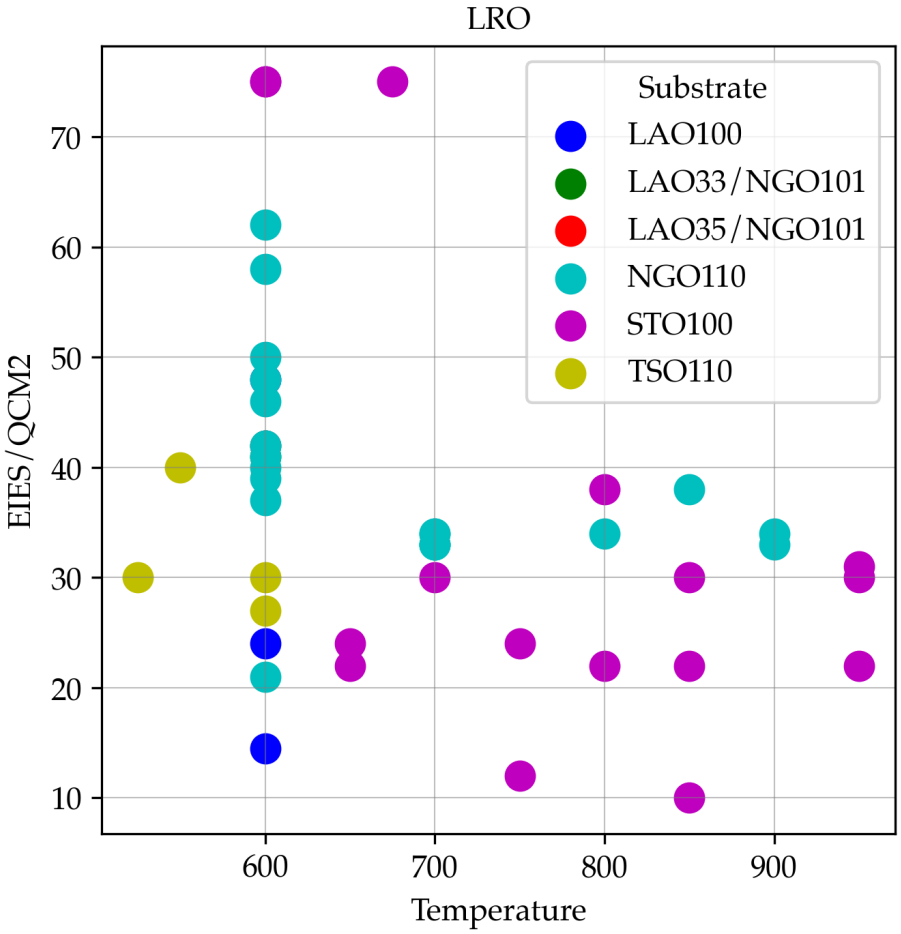

Figure 5. Scatter plot showing the LRO series of growths. Each point indicates a single growth with a particular substrate, substrate temperature, and ruthenium EEIS/QCM2 value corresponding to relative flux.

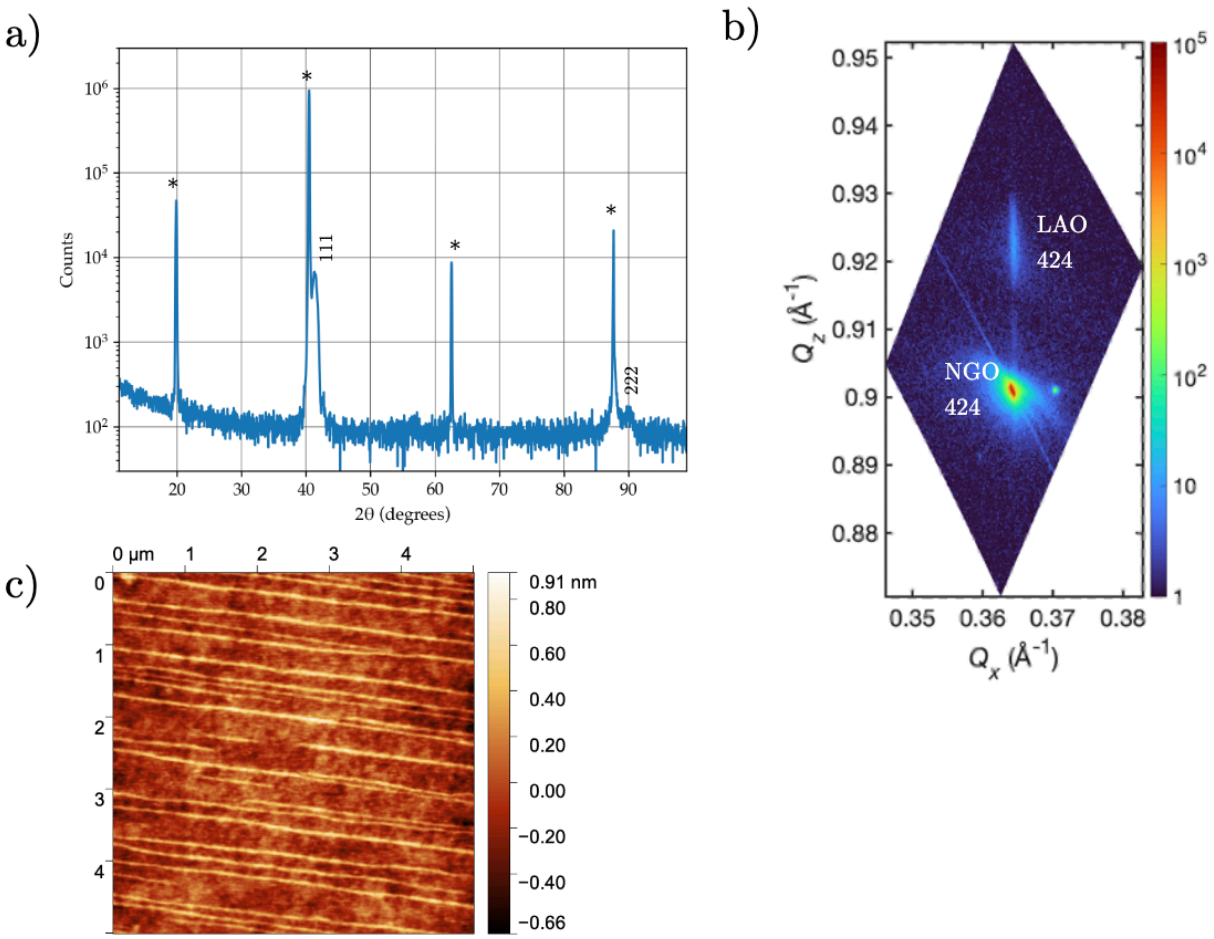

Figure 6. Characterization of sample LAO36. (a) XRD scan of the sample with film and substrate peaks labeled. (b) RSM scan of the sample with film and substrate peaks labeled. (c) AFM image of the sample showing a smooth film with an RMS value of 0.2nm.

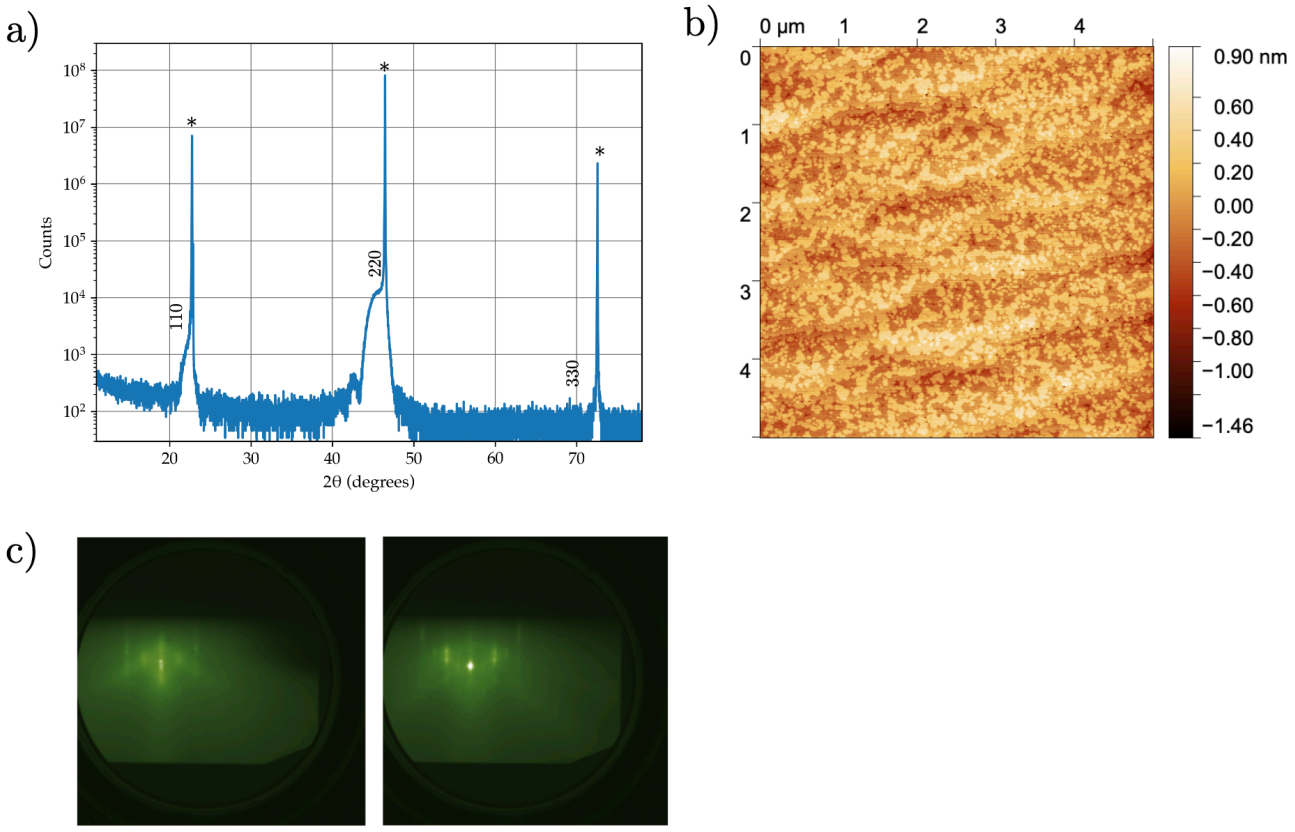

Figure 7. Characterization of sample LRO34. (a) XRD scan of the sample with film and substrate peaks labeled. (b) AFM image of the sample showing a smooth film with an RMS value of 0.25nm. (c) RHEED images of sample showing expected spots and Kikuchi lines.

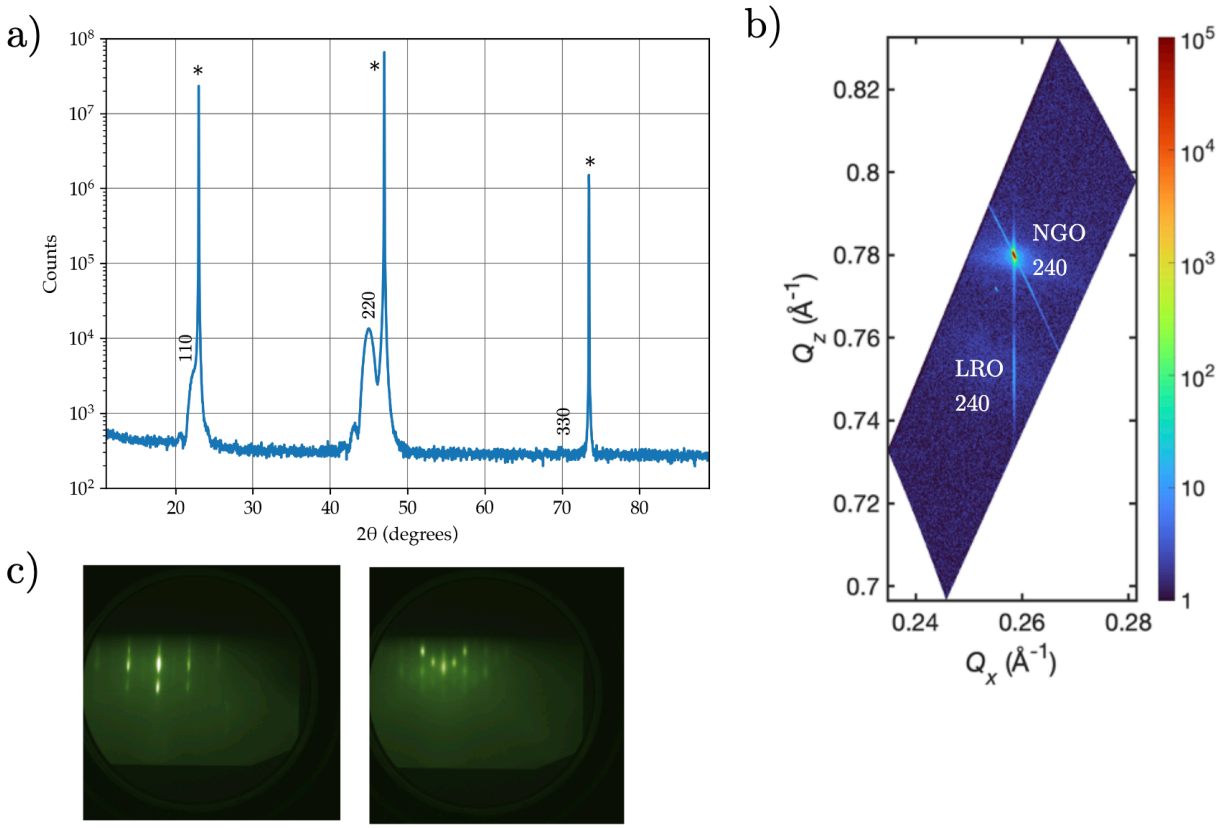

Figure 8. Characterization of sample LRO39. (a) XRD scan of the sample with film and substrate peaks labeled. (b) RSM scan of the sample with film and substrate peaks labeled. (c) RHEED images of sample showing unexpected spots.

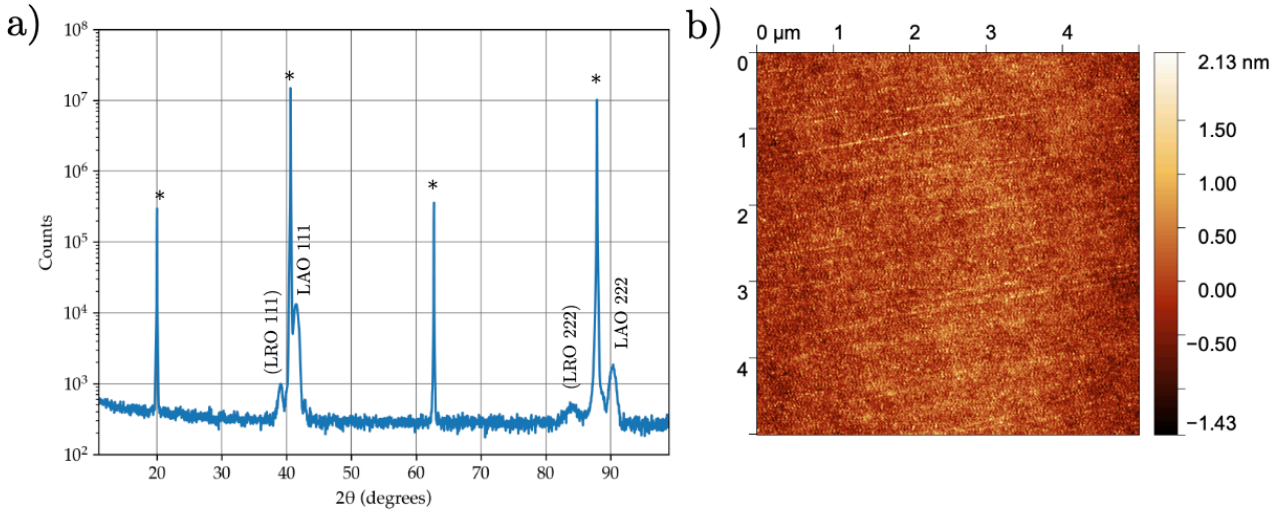

Figure 9. Characterization of sample LRO29/LAO35. (a) XRD scan of the sample with film and substrate peaks labeled. The LAO peaks are located at the expected positions but the LRO peaks may be shifted due to non-stoichiometric phase. (b) AFM image of the sample showing a rougher film with an RMS value of 0.4nm.